Sensors and Materials, Vol. 23, No. 3 (2011) 159–166
MYU Tokyo

S & M 0835

Silicon-on-Insulator-on-Cavity-Structured Micropressure Sensor

Aimin Wu*, Xing Wei, Zhifeng Yang, Jing Chen,
Ming Chen, Dawei Bi, Zhengxuan Zhang and Xi Wang

State Key Laboratory of Functional Materials for Informatics,
Shanghai Institute of Microsystem and Information Technology,
Chinese Academy of Sciences, 865 Changning Road, Shanghai 200050, China

(Received February 9, 2010; accepted July 13, 2010)

Key words: silicon on insulator (SOI), SOI-on-cavity, finite element analysis, pressure sensor

A new design of a micropressure sensor using stress concentration structure, which is fabricated on a silicon-on-insulator (SOI)-on-cavity substrate, is presented in this paper. High sensitivity and good linearity can be achieved simultaneously, and it is fabricated with a larger process tolerance than that by a traditional process. Moreover, it has potential applications in high-temperature environments. Mechanical analysis results and design rules of the structure based on finite element analysis are also presented.

1. Introduction

Silicon on insulator (SOI) has been used more and more widely to improve the performance of micro-electromechanical systems (MEMS) devices, since SOI-MEMS offer several advantageous features in comparison with bulk and surface micromachining.[1–3] A novel SOI-based substrate, which has been called "SOI-on-cavity" substrate, is proposed to provide more freedom for the design and fabrication of SOI-MEMS structures in this paper. Compared with "Si BOX" or "cavity SOI" substrate,[4–7] the SOI-on-cavity substrate is produced by bonding an SOI wafer to a Si wafer with pre-etched cavities, instead of bonding two silicon wafers.

As one of the most successful commercial MEMS products, pressure sensors also benefit from the Si BOX and SOI-on-cavity substrates with low cost and high yield owing to the avoidance of the prolonged back-etching in traditional bulk micromachining.[4–7] However, piezoresistive sensors on Si BOX substrates fail to operate at high temperature owing to the reverse leakage of the p-n junction. By contrast, the SOI-on-cavity substrate has a buried oxide layer acting as an isolation layer for potential applications in harsh environments.[8]

For a flat diaphragm pressure sensor with lateral size a and diaphragm thickness h, a higher sensitivity means a larger a/h, whereas the displacement of the diaphragm is

*Corresponding author: e-mail: wuaimin@mail.sim.ac.cn

directly proportional to a^4/h^4, i.e., the larger the a/h ratio, the larger the displacement, which can lead to severe nonlinearity issues. Severe nonlinearity might make a very sensitive device of little practical value. To solve the dilemma, stress concentration structures[(9–11)] were introduced to design a sensitive pressure sensor with good linearity.

Nevertheless, all these stress concentration structures mentioned in the literature require deep anisotropic etching from the backside, so the feature sizes of the structures could not be defined accurately, i.e., fabrication of the devices requires very tight process control. The pressure sensor demonstrated in this paper combines the SOI-on-cavity substrate and front beam-diaphragm structure. It has all the advantages in nearly all aspects over other existing structures. The design rules based on the results of finite element analysis (FEA) are also demonstrated in this paper.

2. Simulation and Design

A front beam-diaphragm structure is used to reduce the deflection of the diaphragm without loss of sensitivity. Figure 1 is a typical stress contour graph of the beam-diaphragm structure under pressure. It can be seen clearly that the stress is first concentrated from the diaphragm to the beam owing to the thickness difference; then the stress is further concentrated at three narrow regions of the beam owing to the difference in width.

Since the FEA results between the models with and without the oxide layer are no more than 5%,[(12)] it is reasonable to simplify the multilayered SOI structure to bulk silicon model during stress simulation. The stress distribution on the axis line of the beam, simulated in ANSYS, is shown in Fig. 2. The results show that the beam stress

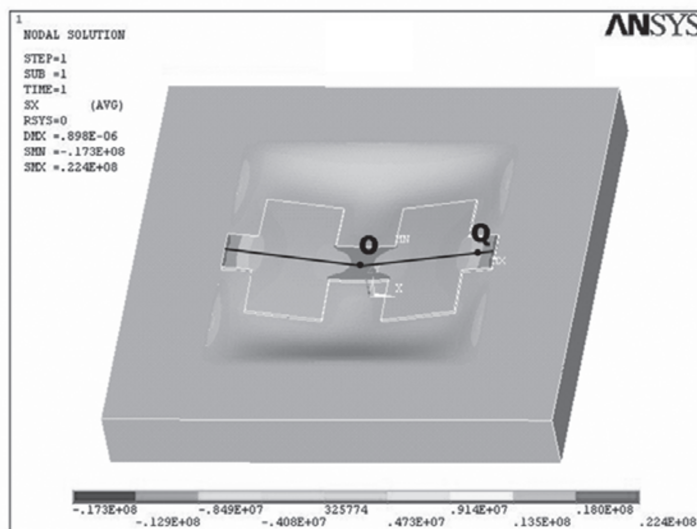

Fig. 1. Typical stress contour graph of the beam-diaphragm structures.

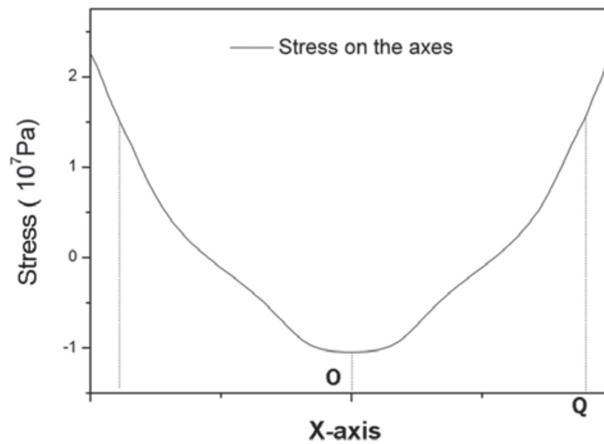

Fig. 2. Stress on the axial line of the beam diaphragm structure.

is concentrated at the three narrow regions. The stress on the central region has a sign opposite to that on the narrow sections at the two ends. Therefore, to design an X-ducer pressure sensor,[13,14] the X-ducer should be put in the center region or the two ends to achieve the largest stress, which corresponds to the maximum sensitivity. Since the beam is made parallel to (110), the axis of the X-ducer should have an included angle at 45° with the beam for the largest output.[15]

To design a beam-diaphragm structure means to choose the optimum geometrical sizes of the beam and the diaphragm. Firstly, the thickness and lateral sizes of the diaphragm are mainly determined on the basis of the pressure range of the device. Thus, there are five remaining parameters of the beam to consider, namely, H, L_1, L_2, W_1, and W_2, as marked in Fig. 3. As the flexure rigidity of the plate is proportional to the cube of its thickness, a difference in thickness by a factor of 2 to 3 often gives a sufficient difference in flexure rigidity for stress adjustment.[16] Thus, H is often defined in this way when the dimensions of the diaphragm are chosen. Then, the effects of the other four parameters, L_1, L_2, W_1, and W_2, on the stress distribution are simulated. When a specific parameter is considered, the other parameters are fixed to a specific value, so the change in the stress at points O (center of the central narrow region) and Q (center of the end narrow region) with the appointed variable could be demonstrated clearly through comparisons.

Since the stress at O has a sign opposite to the stress at Q, the absolute values of O and Q are used in the comparison. Figures 4(a) and 4(b) show that W_1 and L_1 should be made as small as possible for effective stress concentration, as long as the resistors can be accommodated in the narrow regions of the beam. It is shown in Fig. 4(c) that the larger the L_1/L_2 , the larger the stress at Q, while the stress at O is exactly the opposite, which means that L_2 is determined by the position of the X-ducer, around point O or point Q. As for W_2, when the stresses at O and Q reach their peak values, W_2 equals

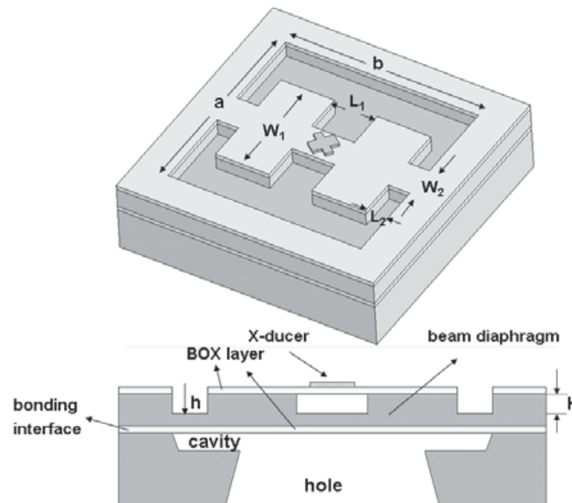

Fig. 3. Schematic of the X-ducer micropressure sensor.

about half the width of the diaphragm, according to Fig. 4(d). Therefore, to obtain the largest sensitivity, W_1 and L_1 should be made as small as possible, and W_2 should be an intermediate value for the X-ducer pressure sensor. L_2 should be made slightly larger than $L_1/2.5$ when the X-ducer is placed at the central region of the beam.

3. Fabrication of the Device

As can be seen from Figs. 5(a)–5(e), the general structure of the pressure sensor is formed by SOI-Si wafer bonding. The original SOI wafer has a 25-μm-thick top Si layer and a 3-μm-thick buried oxide layer. Then, the backside of the top SOI wafer is thinned until 2 microns of the Si layer is left. The pre-etched cavity in the Si wafer is 1,800×2,000 μm^2 with the depth at 25 μm, obtained by anisotropic etching prior to wafer bonding, which can be easily adjusted according to the displacement of the diaphragm for overload protection. Since the hole at the backside is only used for connecting the cavity with the outside, there are no stringent requirements on process control. The beam diaphragm and the X-ducer are sculpted through dry etching of the top SOI structure. The X-ducer is placed at the central narrow region, isolated from the beam diaphragm with the BOX layer. The fabrication flow is finished after the deposition and the patterning of the aluminum electrode.

As for the process tolerance of the device, the SOI-Si bonding and thinning process are very similar to the process of fabricating thick-film SOI wafers, which is mature and reliable. The ultrathin diaphragm, which is crucial to the range and performance of the sensor, is obtained by dry etching the thin top Si layer of the original SOI wafer. Compared with obtaining a several-micron-thick film through prolonged etching of an

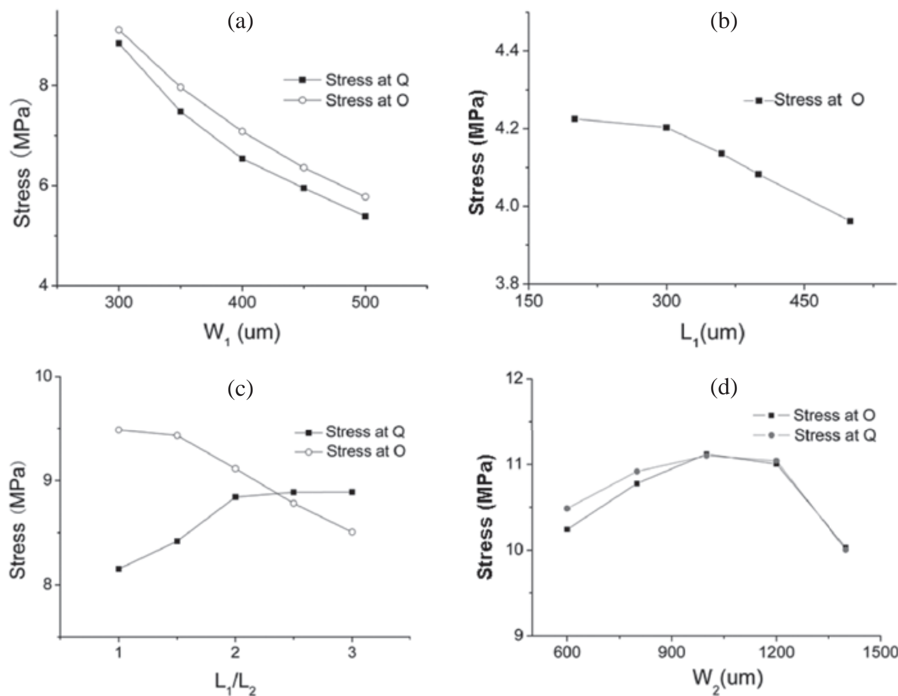

Fig. 4. Stress dependence on specific parameters for a beam-diaphragm structure under 2 kPa pressure with fixed parameters of the beam diaphragm: h = 5 μm, H = 20 μm, a = 1,800 μm, b = 2,000 μm. (a) Stress dependence on W_1 with L_1 = 400, L_2 = 200 μm, W_2 = 1,000 μm; (b) Stress dependence on L_1 with fixed L_1/L_2 = 2, W_1 = 300 μm, W_2 = 1,000 μm; (c) Stress dependence on L_1/L_2 with L_2 = 200 μm, W_1 = 300, W_2 = 1,000 μm; (d) Stress dependence on W_2 with W_1 = 240 μm, L_1 = 400, L_2 = 200 μm.

entire wafer in the structures mentioned above, avoidance of an etching-through issue is much easier, which indicates a larger process tolerance than that of the traditional devices.

4. Results and Discussion

The chip size of the X-ducer micropressure sensor was 3×3 mm^2. The geometric parameters were H = 20 μm, h = 5 μm, a = 1,800 μm, b = 2,000 μm, W_1 = 300 μm, W_2 = 1,000 μm, L_1 = 200 μm and L_2 = 200 μm. The internal structure of the device is shown in Fig. 6. The measurements were performed in a sealed chamber using a Druck DPI610 Portable Pressure Calibrator at room temperature (RT) and 180°C, and 5 V DC was supplied as input. The pressure range used was 2 kPa. For each device, rising and falling turn measurements were carried out ten times to obtain the average sensitivity and nonlinearity, and ten points were selected in each turn. As shown in Fig. 7, the

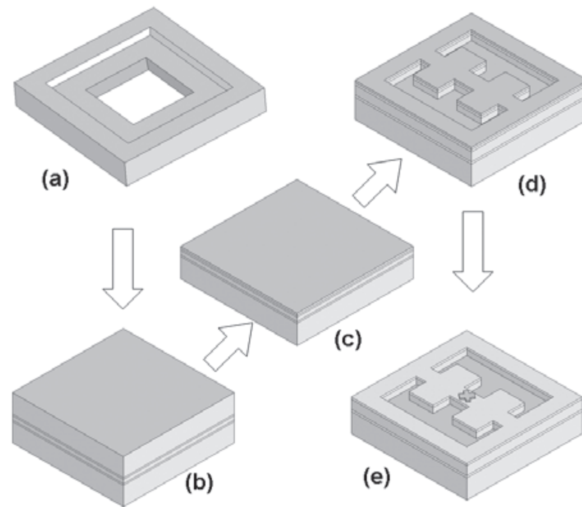

Fig. 5. Schematic fabrication flow of the SOI-on-cavity-structured pressure sensor. (a) Etching to form the cavity and hole; (b) SOI-Si bonding; (c) thinning of the backside; (d) fabrication of the beam-diaphragm structure; (e) schematic of the X-ducer design.

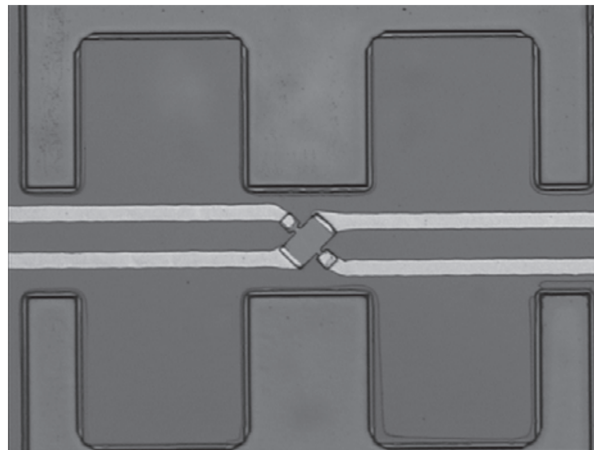

Fig. 6. Internal structure of the X-ducer micropressure sensor.

sensitivity was 3.6 mV/V/kPa at 25°C, and the nonlinearity of the sensor was about 0.51%, which is a fairly good demonstration in comparison with other reports.[17–19] The measurement for high temperature was limited to 180°C owing to the simplicity of the package. The sensitivity was reduced to 2.8 mV/V/kPa at 180°C without loss of nonlinearity. The decrease in sensitivity is considered to be due to the negative effect of the Si piezoresistive factor of varying temperature, which could be adjusted by introducing a temperature compensation circuit.

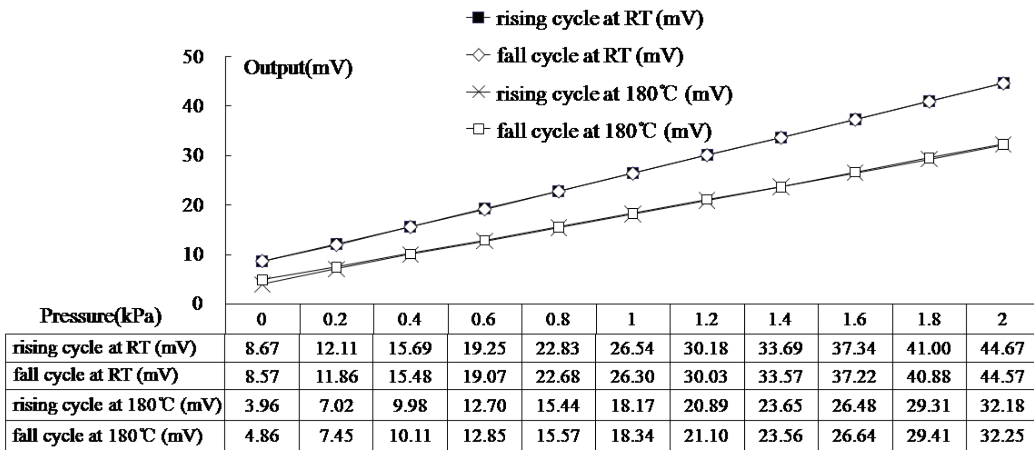

Pressure(kPa)	0	0.2	0.4	0.6	0.8	1	1.2	1.4	1.6	1.8	2
rising cycle at RT (mV)	8.67	12.11	15.69	19.25	22.83	26.54	30.18	33.69	37.34	41.00	44.67
fall cycle at RT (mV)	8.57	11.86	15.48	19.07	22.68	26.30	30.03	33.57	37.22	40.88	44.57
rising cycle at 180℃ (mV)	3.96	7.02	9.98	12.70	15.44	18.17	20.89	23.65	26.48	29.31	32.18
fall cycle at 180℃ (mV)	4.86	7.45	10.11	12.85	15.57	18.34	21.10	23.56	26.64	29.41	32.25

Fig. 7. Mean value of full-scale output for rising and fall test cycle at RT and 180°C.

Furthermore, the pressure range can be conveniently lowered by selecting the appropriate SOI wafer or increasing the dry etching depth, i.e., choosing the proper h and H on the basis of the design rules. The masks are still applicable in this case, which is beneficial to minimize the cost.

The design rules can also be used for Wheatstone bridge pressure sensors. To obtain maximum sensitivity, the four resistors should be made on the three narrow regions of the beam with two at the center and the others at the two ends. For a Wheatstone bridge, the nonlinearity is further affected by the nonlinearity of the resistors, which means that the balance of the stresses in the four resistors has to be considered.

In conclusion, a pressure sensor combining an SOI-on-cavity substrate and a stress concentration structure is demonstrated, realizing high sensitivity and good linearity simultaneously, which can be fabricated with a large process tolerance compared with that by a traditional bulk Si micromachining process. Design rules for the structure based on mechanical simulation results are also presented. Since only parts of the specifications are provided in this article, more characteristics will be investigated to realize a practical industrial product for low-pressure-range applications in harsh environments.

Acknowledgement

This work was financially supported by the National Science Foundation of China (Grant No. 60721004), Science Foundation of Shanghai (Grant No. 10ZR1436100), and the Shanghai Institute of Microsystem and Information Technology Fund for Young Scholars. The authors would like to thank Prof. S. Q. Shen of Fudan University for his help in the measurements.

References

1 V. Mokwa: J. High Speed Electron. Syst. **10** (2000) 147.
2 J. P. Raskin, F. Iker, N. Andre, B. Olbrechts, T. Pardoen and D. Flandre: Electrochim. Acta **52** (2007) 2850.
3 Z. H. Li, Y. L. Hao, D. C. Zhang, T. Li and G. Y. Wu: Sens. Actuators, A **96** (2002) 34.
4 Y. Wang, X. Zheng, L. Liu and Z. Li: IEEE Trans. Electron Devices **38** (1991) 1797.
5 T. Suni, K. Henttinen, J. Dekker, H. Luoto, M. Kulawski, J. Makinen and R. Mutikainen: J. Electrochem. Soc. **15** (2006) G299.
6 J. M. Noworolski, E. Klaassen, J. Logan, K. Petersen and N. Maluf: Transducer 95', Stockholm, Sweden, 25–29 (1995) 71.
7 H. Luoto, K. Henttinen, T. Suni, J. Dekker, J. Makinen and A. Torkkeli: Solid-State Electron., **51** (2007) 328.
8 B. Diem, R. Truche, S. Viollet-Bosson and G. Delapierre: Sens. Actuators, A **21** (1990) 1003.
9 M. Bao, L. Yu and Y. Wang: Sens. Actuators, A **21**–**23** (1990) 137.
10 R. M. Whittier: Endevco Tech Paper, TP277.
11 R. Johnson, S. Karbassi, U. Sridhar and B. Speldrich: Sens. Actuators, A **35** (1992) 93.
12 X. Fu, S. Yao, H. Hou, W. Zhang, Y. Zhao, S. Zhang and W. Zhang: Solid-State and Integrated Circuits Technology Proceedings **3** (18–21) (2004) 1824.
13 Y. Kanda and A. Yasukawa: Sens. Actuators **2** (1982) 283.
14 Motorola Semiconductor Master Guide, Rev. 7 (Motorola, Phoenix, 1994).
15 M. Bao: Handbook of Sensors and Actuators, (8), Micro Mechanical Transducers (Elsevier, Amsterdam, 2004) 222.
16 M. Bao: Analysis and Design Principles of MEMS Devices (Elsevier, Amsterdam, 2005) 291.
17 H. Wang, C. Hsu, W. Liao, L. Yang and C. Dai: MEMS 2006, Istanbul, Turkey, 22–26, Jan. 2006.
18 L. J. Yang, C. C. Lai, C. L. Dai and P. Z. Chang: Tamkang Journal of Science and Engineering **8** (2005) 67.
19 A. V. Chavan and K. D. Wise: IEEE Transactions on Electron Devices **49** (2002) 164.